PCCP

Towards an understanding of the singlet-triplet splittings in conjugated hydrocarbons: Azulene investigated by anion photoelectron spectroscopy and theoretical calculations.

Journal:	*Physical Chemistry Chemical Physics*
Manuscript ID:	CP-ART-03-2015-001826.R3
Article Type:	Paper
Date Submitted by the Author:	13-Aug-2015

Complete List of Authors:	Vosskötter, Stefan; Heinrich-Heine-Universität, Chemsitry, Physical Chemsitry Konieczny, Paul; Heinrich-Heine-Universität, Chemsitry, Physical Chemsitry Marian, Christel; Heinrich-Heine-Universität, Chemsitry, Theor. Chemsitry Weinkauf, Rainer; Heinrich-Heine-Universität, Chemsitry, Physical Chemsitry

Towards an understanding of the singlet-triplet splittings in conjugated hydrocarbons: Azulene investigated by anion photoelectron spectroscopy and theoretical calculations.

Stefan Vosskötter[#], Paul Konieczny[#], Christel M. Marian[§] and Rainer Weinkauf[#]*

Institute of Physical Chemistry; § Institute of Theoretical Chemistry,

Heinrich-Heine-Universität, Universitätsstrasse 1, 40225 Düsseldorf.

E-mail address: Weinkauf@uni-duesseldorf.de

In this work, the relative energetics and the character of singlet and triplet states of azulene have been investigated by photodetachment photoelectron spectroscopy (PD-PES) at radical anions and high-level multi-reference configuration interaction (MRCI) theory. Anion-to neutral electronic transition energies and singlet-triplet splittings have been measured directly by PD-PES and have been assigned with the help of the calculated transition energies and simulated Franck-Condon spectra. The good agreement between experiment and theory justifies the conclusion that the geometrical structure of the azulene radical anion lies in-between the geometries of the neutral ground state and those of the excited states. By the detour via the radical anion, we observed the T_1 and S_1 origins of azulene in the same spectrum for the first time and were able to resolve their small splitting of 49 meV. This small singlet-triplet splitting was explained before by the small overlap of the electron densities in the highest occupied and lowest unoccupied orbital. In this work, this concept is generalized and applied to the higher excited electronic states of azulene as well as to its alternant aromatic isomer naphthalene. The results confirm our hypothesis that the energetic splittings of corresponding singlet-triplet pairs can be related to the degree to which the electron density distributions of the involved half-occupied orbitals overlap.

*To whom correspondence should be addressed

1 Introduction

Triplet states play a crucial role in the photophysics and photochemistry of many chromophores.[1,2] The first excited triplet state (T_1) of a typical organic compound is longer-lived than its singlet counterpart (S_1). It can therefore initiate intermolecular processes such as chemical reactions, spin transfer or charge transfer.[1] For example, in solution molecular oxygen often has the time to approach a triplet-excited molecule by diffusion. Energy and spin transfer quenches the triplet excitation and generates reactive oxygen species. In the solid state, the role of triplet states can be even more complex. In crystalline tetracene samples, e.g., triplet states on neighboring molecules can be generated (singlet fission) or annihilated (triplet fusion) by efficient spin-allowed intermolecular excitation energy transfer processes.[3]

Triplet states can be important intermediates of photophysical pathways in isolated molecules, too. In heteroaromatic compounds, for example, fast radiationless transitions from S_1 to adjacent triplet states by intersystem crossing (ISC) can efficiently quench the fluorescence. Since phosphorescence emission from T_1 at room temperature is typically very inefficient in organic compounds[1], triplet states are considered as dark states in optical spectroscopy.

Triplet states play also an important role in molecular electronics. For example, the electron-hole charge recombination process, the key process in organic light emitting devices (OLED), involves triplets. In this process, besides the S_1 population, also a strong T_1 population is created.[2] In conventional electrofluorescent materials, this triplet branch is "dark" and relaxes radiationlessly. Hence, triplet generation constitutes a severe limitation for the luminescence efficiency of first-generation OLEDs.[2] In second- and third-generation organic electroluminescent materials, the triplet population is harvested either as phosphorescence by adding heavy atoms, such as transition metals, thus enabling delayed luminescence.[2]

In order to understand the photophysics and photochemistry of an organic compound in detail, it is important to know at least the relative energetics of the low-lying singlet and triplet states. For many molecules, however, especially the higher excited triplet states are still unknown. It is even very difficult to predict the number of triplet states located below S_1 and their energy separation. Three examples may illustrate this problem. In fluorine, six triplet states lie below the S_1 state[4] whereas in cycl[3.3.3]azine the T_1-S_1-splitting is predicted to be very small and possibly T_1 may be even above the S_1.[5] Even worse, in a simplistic approach it is assumed that the singlet-triplet splitting of the lowest excited states in a molecule always corresponds to the T_1-S_1 energy difference. A careful analysis of the electronic structure of naphthalene, for example, shows that the excitation from the highest occupied molecular

orbital (HOMO) to the lowest unoccupied molecular orbital (LUMO) gives rise to the T_1 and the S_2 (B_{2u}) pair of states whereas the S_1 state (B_{3u}) correlates with the T_2 state.[6] Hence, in naphthalene the singlet-triplet splitting of the HOMO-LUMO excitation is 1.8 eV and not 1.37 eV which is the T_1-S_1 energy difference.[6] Already these few examples show that the relative energetics of singlet and triplet states obviously do not follow simple rules and cannot be understood without theoretical calculations.

In this work, by a concerted action of experiment and theory, we try to shed some light on singlet-triplet splittings. Our goal is to find general aspects allowing at least a qualitative understanding of the irregularities observed in the singlet-triplet splittings of organic conjugated molecules. To this end, we measure the singlet-triplet state splitting of T_1-S_1, but also the singlet triplet splitting of corresponding higher excited states and correlate them by theoretical calculations with properties of the involved molecular orbitals.

Azulene was chosen as sample molecule because of its many exceptional properties. For example, it has an unusually small T_1-S_1-splitting but importantly also a positive electron affinity (EA). The positive EA is needed for the application of photoelectron spectroscopy to the radical anion of azulene. Anion photoelectron spectroscopy or photodetachment photoelectron spectroscopy (PD-PES) is one of the few experimental gas-phase spectroscopy methods which provide comparable yields for singlet and triplet state excitations.[7, 8] It is thus particularly well suited for investigating singlet-triplet state splittings, especially of higher excited states.

For the chemical structure of azulene and its isomer naphthalene, see Figure 1. The concept to mark atoms by stars, as shown in Figure 1, has been introduced by Coulson and Rushbrooke[9] and continued later by Dewar and Dougherty[10] in order to classify alternant and non-alternant conjugated hydrocarbons. If, for example, stars are given to the atoms at the end of each double bond (in a counter-clockwise turn) a conjugated hydrocarbon molecule is termed alternant if all starred atoms have only un-starred neighbor atoms and *vice versa* and non-alternant otherwise. According to this definition, azulene (see Figure 1 b) is a non-alternant hydrocarbon because there are two un-starred neighboring atoms at the transannular bond whereas its isomer naphthalene (Figure 1a) is an alternant hydrocarbon. Unfortunately, naphthalene does not have a positive electron affinity, so that a direct comparison of the two iso-atomic conjugated hydrocarbons by anion PD-PE spectroscopy is not possible. In order to examine whether the concepts developed in the following for azulene also hold for

naphthalene, we carried out quantum chemical calculations for both molecules at the same level. The result of this comparison is presented and discussed in Section 4.

In the following we give a short introduction to the theoretical background concerning singlet-triplet splittings. In molecules in which the excited singlet-triplet pair is characterized by the excitation of an electron from an occupied molecular orbital Ψ_a to an unoccupied molecular orbital Ψ_b, the S-T splitting is approximately equal to two times the value of the exchange integral K_{ab} of the unpaired electrons where K_{ab} is defined as [11,12,13]

$$K_{ab} = \iint_{-\infty}^{+\infty} \Psi_a(\vec{r}_1) \cdot \Psi_b(\vec{r}_2) \frac{1}{r_{1,2}} \Psi_b(\vec{r}_1) \cdot \Psi_a(\vec{r}_2) d\tau_1 \cdot d\tau_2 \qquad \text{(Equation 1)}$$

Among theoreticians it is well known that the size of this exchange integral K_{ab} depends exponentially on the distance of the unpaired electrons.[11,12] This exponential distance dependence of K_{ab} has its origin in the fact that the atomic wave functions from which the molecular wave function is constructed decay exponentially with the distance from their centres.[11,12] In practice this means that S-T splittings are expected to be small or very small in such cases where the distance between the charge centres of Ψ_a and Ψ_b is large. Very obviously this is the case for charge-transfer states. A small overlap of the orbital density distributions is also typical for nπ* and Rydberg. For a detailed discussion on S-T splittings of nπ* and charge-transfer excitations see for example Ref. 2. With regard to the S-T splitting of ππ* excitations, this simple concept has to be extended, however. Klan and Wirz[11] explicitly address the consequences of disjunct and non-disjunct atomic electron densities in the HOMO and the LUMO orbitals of aromatic hydrocarbons. They show that very small S-T splittings can be achieved also in such molecular systems where the centres of the electron clouds in the HOMO and LUMO are not or nearly not displaced with respect to each other, but the local electron densities in HOMO and LUMO peak at different atoms and are disjunct. This "disjunct" situation was assumed to apply especially for the T_1 and the S_1 states of azulene.[11] One of the questions we address in this work is whether this "disjunct" situation is typical for all singlet-triplet pairs in azulene or not and whether such situations do also occur in alternant hydrocarbons such as naphthalene.

Azulene became famous not for its small T_1-S_1 energy gap, but because it was the first and for a long time the only molecule which was proven to violate Kasha's rule.[14] This rule states that fluorescence is always emitted from the lowest excited singlet state. For azulene, an anomalous S_2 fluorescence, but no S_1 fluorescence was observed at first.[15,16] The existence of the S_2 fluorescence was explained by a relatively slow internal conversion caused by the

unusually large S_1-S_2 energy gap.[17,18] Later it was shown that there is also a very weak S_1-S_0 fluorescence and that one reason for its small intensity[18] is the short S_1 lifetime as determined in the gas phase by line width (0.9 ps at the S_1 origin transition)[19] and pump-probe measurements (0.9 ps at about 2000 cm^{-1} of vibrational energy in S_1).[20] Theoretical calculations suggested that the short S_1 lifetime is caused by a conical intersection of the S_1 state with the ground state.[21,22] Ruth et al. later recalculated lifetimes from line widths taken from a gas phase absorption spectrum of cold azulene molecules.[23] Their substantially longer lifetimes (for example 2.6 ps at the origin)[23] result from a new fitting procedure in which they explicitly included the underlying rotational band contours of the transitions. In this investigation also a step-like increase of the S_1 line width above a vibrational energy of 2100 cm^{-1} was observed. This value nicely agrees with the threshold (2300 cm^{-1}) for the conical intersection found in femtosecond pump-probe measurements in solution.[24] A subsequent theoretical study was able to reproduce these experimental S_1 lifetimes by internal conversion (IC) to S_0.[25] All data agree that the conical intersection between the S_0 and the S_1 state takes place at high internal S_1 energy.

The vibronic structure of the experimental S_0-S_1 absorption spectrum, which extends over five thousand wavenumbers, was well reproduced by Franck-Condon simulations based on TDDFT calculations.[25,26] Because the permanent dipole moment changes during the S_0-S_1 transition, the S_1 state of azulene was sometimes drawn as a bi-radical (see for example Ref. 21).

Concerning the triplet states, Nickel et al. tentatively attributed a delayed, red-shifted photoemission in a cooled azulene-doped phenazine host crystal to the phosphorescence of azulene (tentative origin of the T_1-S_0 transition at 1.711 eV).[27] In the same publication[27] and a subsequent paper,[28] it was also postulated that the triplet lifetime is shortened by a temperature-induced reverse intersystem crossing from T_1 to S_1, which is then predominantly followed by a fast non-radiative S_1 decay. This process was observable because a small fraction of this indirectly populated S_1 state emitted photons which could be detected due to their delayed appearance.[28]

In the gas phase, the electron affinity (790 ± 8 meV)[29] and the origin energies of the S_1 (1.771 eV)[19,23] and the S_2 (3.565 eV)[30] states are already published. The latter two are important for the assignment of the singlet state transitions and to verify the calibration of our PD-PE spectra (see Section 3). No band corresponding to the T_1 state was found in electron energy loss spectra, which is usually very sensitive for triplet states.[6] The authors explain this by the

very small T_1 to S_1 state spacing, which was experimentally not resolvable. In the same work, a new band at 2.82 eV (onset) was assigned to a higher excited triplet state on the basis of theoretical data[31] and another transition at 4.22 eV was identified as S_3.[6] Recently by benchmark theoretical studies the EA (0.71 eV) and the transition energy to T_1 (1.79 eV) of azulene was calculated.[32]

In this work, we present experimental and theoretical data for singlet and triplet state energies of azulene and analyze dipole moments, electron configurations and wave functions of the most relevant electronic states. We discuss singlet-triplet splittings for the T_1-S_1 pair as well as for some higher excited singlet-triplet pairs and compare the observed trends in azulene with our theoretical findings for naphthalene.

2 Experimental and theoretical methods

2.1 Theoretical methods

All geometry optimizations were performed using the TURBOMOLE 6.3 program package.[33] DFT in conjunction with the B3-LYP functional was used for the neutral ground state S_0 of azulene and naphthalene while unrestricted DFT (UDFT) was utilized for the radical anion ground state D_0 of azulene.[34, 35] Time-dependent DFT (TDDFT) was applied for the geometry optimization of the electronically excited states of neutral azulene.[36] On all atoms the atomic orbital basis comprised TZVPP basis sets from the TURBOMOLE library.[37] The adiabatic EA has been calculated as energy difference between the geometry-optimized anion ground state and the geometry optimized neutral ground state including zero-point energies. Vibrational frequencies were determined by numerical differentiation using the SNF program.[38] Franck-Condon (FC) spectra were generated for the anion state D_0 as the initial state and the states of the neutral molecule as final states with a recent version of the VIBES program.[39] The time correlation function was damped by a Gaussian of width 50 cm^{-1} and evaluated at 2^{16} grid points in a time interval of 300 fs. The FC spectra are then obtained by fast Fourier transformation. For details see Ref. 39.

At all optimized geometries, electronic excitation energies and wave functions were calculated using the DFT/MRCI method.[40] The molecular orbital (MO) basis for the DFT/MRCI expansion was generated by closed-shell DFT calculations using the BH-LYP functional.[35,41] Maintaining the C_s symmetry constraints, we determined the ten lowest ^{1}A' and ^{3}A' states of azulene and one state of singlet and triplet multiplicity, respectively, in the A'' irreducible representation. For the D_{2h} symmetric naphthalene, we only carried out

calculations at the neutral ground-state geometry where we optimized MOs and determined energies and electron configurations for 4 A_g, 4 B_{1g}, 4 B_{2u}, and 4 B_{3u} states of singlet and triplet multiplicity, respectively.

2. 2 Experimental setup

Azulene was purchased from Sigma and used without further purification. Our anion photoelectron spectrometer consists of four vacuum chambers for i) anion formation, ii) ion acceleration, iii) mass selection by linear time-of-flight mass spectrometry and iv) PD-PE spectroscopy in a time-of-flight photoelectron spectrometer.

The sample molecules sublimate in a heated (80 °C) and pulsed nozzle. The Ar backing pressure in the nozzle is typically 10 bar. The Ar carrier gas and a small percentage of sample are co-expanded into the first vacuum chamber and form a supersonic expansion, which internally cools the sample molecules. For electron beam generation we use a stack of micro-channel plates (MCP) seeded with UV-light.[42] In the expansion, the injected high-energy primary electrons form low-energy secondary electrons, which can efficiently attach to sample molecules. Their internal vibrational energy, as caused by the electron attachment, cools in the ongoing expansion. The supersonic beam is skimmed and introduced into the first field-free ion extraction zone in a second vacuum chamber. A delayed, time-synchronized high voltage pulse accelerates the anions to an energy of about 300 eV into the linear time-of-flight mass spectrometer and on a MCP detector for mass analysis. Typically, no dissociation products are observed in our anion mass spectra. For photodetachment (PD) a pulsed Nd:YAG laser (Innolas, Spitlight 600, 5 ns pulse width, 1064 nm and higher harmonics) hits the ions 15 cm before the mass detector. The light pulse performs PD of the mass-selected anions in a field-free μ-metal tube. The electrons emitted in the right angle are detected in a MCP detector and their flight time is measured by a LeCroy oscilloscope (Type: Waverunner 64 xi). The electron energy resolution depends primarily on the kinetic energy of the electrons. We therefore recorded PE spectra with the different harmonics of a Nd:YAG laser (1064 nm, 532 nm, 355 nm, 266 nm, 212.7 nm). For each detachment wavelength we can shift one or two transitions of interest into the electron energy range of optimal energy resolution. With this procedure, the electron energy resolution in our PE spectra is at best 5 meV, but typically 5-10 meV. The absolute accuracy in electron energy was calibrated by using atomic iodine and is ± 5 meV.

Because the electronic states have been recorded with different excess energies, the intensities of the electronic transitions are affected differently by threshold effects of the detachment processes.[43] In addition, resonant excitations to anion excited states can occur, which can be followed by electronic and vibrational state-selective autodetachment.[44] This means that in our PD-PE spectra relative intensities of electronic transitions are reliable only in those cases, in which the electronic states are energetically close to each other and have similar electronic structures. Since the ionization energy of azulene[45] is known, we also checked whether there are photoelectron peaks in our PE spectrum which could result from two-photon process: For example, the first photon excites the S_1 or T_1 state of the neutral molecule and the second photon ionizes from S_1 or T_1 to the radical cation. No evidences for such two-photon processes have been found.

3 Results

In this Section, we present the PD-PE spectrum of azulene and compare the measured electronic state energies to our theoretical results and previously published data. The detailed analysis of the theoretical results and the consequences thereof are discussed in Section 4.

The overview PE spectrum of azulene is shown in Figure 2. It is composed of sections a) – e) which are slices of a set of PE spectra recorded each with a different detachment wavelength: a): 1064 nm, b): 532 nm, c): 355 nm, d): 266 nm and e): 212.7 nm (for explanations see Section 2.2). The spectrum in inset f) was recorded with a higher anion current and suffers from low electron energy resolution due to Coulomb interaction between the electrons with the negative anion cloud.

The energy scale at the bottom starts at the anion ground state and the energy scale at the top with the neutral ground state. If not otherwise stated, in the following energies are given in eV with respect to the origin transition of the neutral S_0 state.

The PE spectrum of azulene in Figure 2 shows the transitions from the anion ground state D_0 to the ground state S_0 of the neutral molecule, to the two close-lying states T_1 and S_1 and to the states T_2, T_3, S_2 and T_4. The S_0 position in the energy scale at the bottom provides the EA of azulene (0,790 eV) which is in good agreement to a former experimental value (0.790 eV)[29] and theoretical calculations of others (0.79 eV)[32] and calculations performed in this work (0.65 eV). The origin transitions to the S_1 and S_2 states are identified in the PE spectrum by comparison to published highly accurate gas phase transition energies (S_1: 1.771 eV[19,23], S_2: 3.565 eV[30]). Since the absolute accuracy of the photoelectron energy in our PE spectrum is

better than ± 5 meV, the assignment of the second peak in the inset g) of Figure 2 to the origin transition of the S_1 state is beyond doubt. As a consequence, there is no other choice as to assign the peak closely below the S_1 origin (1.771 eV) to the origin transition of the T_1 state (1.722 eV). This gives a T_1-S_1 splitting of 49 meV. The assignment of T_1 and S_1 in our PE spectrum is also supported by the calculated absolute energies of T_1 and S_1 (this work: T_1: 1.758 eV; S_1: 1.827 eV), the calculated T_1-S_1-Splitting (69 meV) and Franck-Condon simulations which predict strong origin transitions for T_1 and S_1 and only small intensities for vibronic transitions (see below). We hence believe that our assignment of the T_1 state is grounded on conclusive arguments.

The two transitions at 2.380 eV and 2.852 eV are broad and weak. To enhance the signal-to-noise ratio for these transitions they have been recorded in addition with a much higher anion current. This provides higher electron intensities but reduces the electron energy resolution due to Coulomb effects (see inset f) in Figure 2). These two transitions are attributed to T_2 and T_3 by comparison to their calculated state energies (2.264 eV and 2.701 eV). The transition to T_3 also agrees well with a triplet state found in electron energy loss spectra at 2.82 eV.[6] The T_2 state is somewhat broader than the T_3 state (see inset f) in Figure 2). This may be caused by a broad vibronic pattern and a superimposed lifetime effect: The geometry optimization of the T_2 state leads without barrier to a conical intersection with the T_1 state (see Section 4). The transition at 3.863 eV, 300 meV above the S_2 origin, (see Figure 2 and 3b) agrees well with the calculated energy for the T_4 state (theory: 3.871 eV). An assignment to a vibronic transition of S_2 is highly implausible as the Franck-Condon simulations presented in the following section show.

All electronic transitions in the PD-PE spectrum presented in Figure 2 show strong origin transitions and a short vibrational progression. This is in sharp contrast to the S_0-S_1 absorption spectrum in the gas phase[23,25] which extends over five thousand wavenumbers. In order to obtain a deeper understanding for the geometry effects in the anion PD-PE spectra we performed FC simulations from the anion ground state to the electronic states of the neutral molecule. In Figures 3 a)-d), the experimental and the calculated FC spectra from the anion to the S_0 (a), the S_2 (b), T_1 and the S_1 states are shown. Note that the calculated vibrational frequencies have not been adapted by calibration. For the close-lying states T_1 and S_1, in Figure 3 d) the origins of the two calculated spectra are shifted against each other by the experimentally found T_1-S_1 energy splitting (49 meV) and then added. Note especially the very good agreement between the calculated and measured spectra for the transition to the S_0

state (Figure 3 a)). The vibronic transitions 1-5 nearly perfectly correspond to each other in position and intensity. For the transition to S_2 (Figure 3 b)), the vibronic transitions 1, 2 and 3 in the experimental spectrum are also well reproduced by theory. The transition at 298 meV (2433 cm^{-1}) above the S_2 origin is not present in the simulation. This supports our assignment of this transition to the electronic origin of the T_4 state (see above).

In Figure 3d) the theoretical (spectrum at the top) and experimental (spectrum at the bottom) PE spectra contain the superimposed vibronic transitions of the states T_1 and S_1. The intensity ratios between the origin transitions and the vibronic transitions in the simulated spectrum are very similar to those in the experiment spectrum. Note, however, that the vibrational energies in the experimental spectrum are somewhat lower than the calculated vibrational energies. This evidences the deficiencies of the harmonic approximation for these low-frequency modes. One would think that the peaks 1-5 in Figure 3d) are resolved vibrations of T_1 or S_1. A comparison of the peak positions from our PE spectrum with transition energies of the gas phase S_0-S_1 absorption spectrum[23] is, however, very difficult. If the vibrations in T_1 have similar energies and intensities as those in S_1 – which is very likely because of the large similarity of the corresponding electronic wave functions – then by accident most of the observed peaks would contain several transitions which are not resolved. We believe to find evidences for the presence of vibrations 15^1_0 and 13^1_0 in S_1 and 16^1_0, 15^1_0 and 13^1_0 in T_1 (vibrational numbering and frequencies see Ref 23).

In conclusion, the nearly diagonal FC factors for all electronic transitions in azulene suggest that the geometry of the anion ground state lies in-between the geometries of the ground and the excited states of the neutral molecule. This is an important result, because it gives us the hope that also for other aromatic molecules the PD-PE spectra might be not too crowded with peaks.

4 Discussion

In this section, we present further theoretical results for azulene and naphthalene which give deeper insight into the shape of the excited-state surfaces and more general aspects of the singlet-triplet splittings of higher excited states.

Calculations of excited state surfaces

Whereas for S_0 and S_2 the calculated Franck-Condon spectra agree with the experiment concerning intensity and vibrational frequencies (see Figure 3 a) and 3 b)), for T_1 and S_1 the

calculated vibrational energies are too high in comparison to those found in the PE spectrum. This deviation is an indication that the molecular potential energy surface along these nuclear coordinates is shallower than calculated. When we investigated this more in detail, we found that TDDFT provides a T_1 double minimum structure in which the twofold rotational symmetry of azulene is destroyed leading to bond alterations in the rings. Pointwise MRCI calculations along this distortion coordinate show, however, that the geometry is still C_{2v} symmetric at this level of theory but that the potential is very flat. This is very much in agreement with a comment of Semba et al. made in a mostly experimental paper.[30] These authors proposed that the S_1 surface has a shallow potential and that this shallowness could considerably contribute to the differences between the S_2-S_1 and S_1-S_0 IC rates.[30]

Our geometry optimizations of the higher excited-state structures revealed a conical intersection of the T_2 with the T_1 state. In Figure 4, we have plotted DFT/MRCI single-point energies calculated along an interpolated path connecting the S_0 ground state minimum (x = 0.0) with the geometry at which the conical intersection between T_1 and T_2 takes place (1.0) at the TDDFT level. Note that the crossing between T_2 on the one hand and T_1 and S_1 on the other hand takes place at a more distorted geometry (x = 1.75) at the DFT/MRCI level than at the TDDFT level. Note also that the T_1 and S_1 potentials are very close and run almost parallel to each other along the investigated path. Because of this small T_1-S_1 energy difference, the slightest distortion of the nuclear framework along one or more reaction coordinates would immediately lead to a crossing of the two potential energy surfaces. This could explain why a reversed ISC from T_1 to S_1, as found experimentally,[27,28] can occur with a reasonable efficiency.

The singlet-triplet splittings

The good agreement between the measured and the calculated transition energies (see Table 1) shows that our theoretical methods are able to describe higher excited states with high accuracy, too. Hence, in the following we will also discuss electronically excited states which have not been observed experimentally.

An interesting question is, what causes the small T_1-S_1 singlet-triplet splitting in azulene. A detailed theoretical analysis of the charge distributions of S_0 and S_1 in azulene shows that the dipole moment changes only slightly when the molecule is excited from S_0 ($\mu \sim 0.8$ Debye) to S_1 ($\mu \sim 1.2$ Debye, but with a reverse direction in comparison to S_0). This means that the S_0-T_1 and S_0-S_1 excitations do indeed shift some electron density from the five-membered ring to

the seven-membered ring, but that this charge transfer is small and cannot account for the small T_1-S_1 splitting.

The conclusive explanation for the small T_1-S_1 splitting dates back to Klan and Wirz.[11] Molecular orbital theory implies that the unpaired electrons in the S_1 and T_1 states are located in the LUMO and HOMO, respectively. This statement might sound trivial, but the excitation energies of electronic states are not solely determined by orbital energies but also by two-electron interactions. In azulene, the HOMO-LUMO excitation indeed dominates the wave functions of the S_1 and T_1 states. But, as we will show below, this is not the case in the isomeric alternant hydrocarbon naphthalene.

Our calculations confirm the hypothesis of Klan and Wirz [11] that the electron densities of these two orbitals are almost disjunct for the non-alternant hydrocarbon azulene, but typically overlap strongly for alternant hydrocarbons, such as for example naphthalene. In azulene, the electron densities of the calculated LUMO (Figure 5 b)) and HOMO (Figure 5 c)) peak at different atoms. As a consequence, the exchange integral which largely determines the singlet-triplet gap is very small. Indeed, the experimental value of merely 49 meV matches well this theoretical expectation. Please note that for the electron densities the signs of the wave functions are of no importance.

In the following, we apply the electron density-overlap concept to the T-S splittings of higher excited electronic states. As can be seen in Table 1, most of the higher-lying excited states of azulene exhibit some multi-configurational character, thus slightly complicating the line of arguments. For example, the T_2 wave function has a coefficient of 0.91 for the $(H\text{-}1)^1L^1$ configuration and a coefficient of -0.27 for the $H^1(L+1)^1$ configuration. The best corresponding singlet state would be the S_2 state with coefficients of 0.70 for $(H\text{-}1)^1L^1$ and of -0.60 for $H^1(L+1)^1$ (see Table 1). A comparison of the relevant orbitals (Figure 5 b/d and 5 a/c) shows that they have all strong electron density overlaps at the same atoms. This is in qualitative agreement with the relatively large measured and calculated T_2-S_2 splitting values of 1.185 eV and of 1.195 eV.

Another correlated singlet-triplet pair would be T_3 and S_4 of azulene. They have the same configurational contributions ($H^1(L+1)^1$ and $(H\text{-}1)^1L^1$), however with very different coefficients. Both MO pairs have good electron density overlap (see Figure 5 a/c and b/d) in agreement with a relatively large splitting of 0.9 eV. It further seems that T_4 and S_3 constitute a correlated singlet-triplet pair, since they share the same excitations, i.e., $(H\text{-}1)^1(L+1)^1$ and

$(H\text{-}2)^1L^1$. The MO densities of these orbitals have some but no perfect overlap (compare Fig 5 a/c and b/e). This alone would predict a medium-sized singlet triplet splitting in agreement with the calculated splitting of 255 meV. This analysis shows that the very small S_1-T_1 splitting is an exception also for azulene.

In order to test whether the concept of electron density overlap is also applicable to alternating hydrocarbons we calculated wave functions (see Figure 6) and electron configurations for the T_1, T_2, S_1 and S_2 states of the alternating hydrocarbon naphthalene. As mentioned in the introduction, in naphthalene T_1 correlates with S_2 (both states have mostly H^1L^1 configurations (coefficient of the two configurations in both states: 0.39). A comparison of Figure 6 b) (LUMO) and c) (HOMO) reveals that the electron density overlap is strong: The wave functions peak at the same atoms. This nicely correlates with the experimentally observed singlet-triplet splitting of 1.8 eV.[6] Interestingly, in naphthalene the T_2 state correlates to S_1 (both have equal contributions of $(H\text{-}1)^1L^1$ and $H^1(L+1)^1$ configurations (coefficient of each configuration 0.7)). A comparison of the H-1 and L and of the H and L+1 orbitals shows that the electron densities in the half-occupied orbitals have relatively small overlap in agreement with the small T_2-S_1 energy difference of 130 meV.[6] The example of naphthalene suggests that also in alternant conjugated hydrocarbons the electron density overlaps between the involved orbitals can cause very different singlet-triplet splittings in the same molecule.

Our analysis qualitatively explains why the energetic spacing of the ladder of triplet states is very rarely similar to the ladder of the singlet states. Note that the simple overlap rule might in general be difficult to apply for higher excited states because, as Table 1 shows, the wave function contributions in a singlet-triplet pair do not perfectly match in size anymore. In addition, the wave functions adopt more and more multi-configuration character with increasing excitation energy. On the one hand this configuration mixing prevents the unambiguous assignment of corresponding singlet-triplet pairs and on the other hand should in general favour the case where the overlaps of the wave functions are not very small. For statistical reasons, the probability of fully disjunct electron densities should decrease with the number of configurations mixed into a state.

5 Conclusion

In conclusion, with PD-PES we have directly measured energies of singlet and triplet states and singlet-triplet energy gaps in azulene. With the help of calculated anion-to-neutral transition energies and Franck-Condon simulations, we could assign the measured transitions. These results suggests that in general for conjugated molecules the geometrical structures of their radical anions lie in-between these of the S_0 states and the higher excited states of the neutral molecules. Thus, predominant origin transitions are expected to be a general signature of PD-PE spectra of the excited states also for other conjugated molecules of photochemical interest.

A detailed theoretical analysis of the electronic structures of the excited electronic states confirms previous statements[10] that the T_1-S_1 splitting is small due to small HOMO-LUMO electron density overlap. In contrast, for all higher excited states of azulene investigated in this work, the electron density overlaps of the involved orbitals are substantial and cause large triplet-singlet state splittings, comparable in size to the T_1-S_1 splittings typically observed in alternant conjugated hydrocarbons. Our analysis of the electronic structures of the excited electronic states further shows that i) the knowledge of the electron configurations of the electronic states is essential in order to properly assign corresponding singlet-triplet pairs, ii) that only then the corresponding wave functions can provide a rough estimate of the electron density overlap of the involved half occupied orbitals and iii) that this overlap can be used to qualitatively understand the singlet-triplet splittings. The importance of i) is illustrated by the naphthalene example: In naphthalene, the T_1 state correlates with the S_2 state and not with the S_1 state as one may assume without knowing the electron configuration. The substantial singlet-triplet splitting of the HOMO-LUMO transition of naphthalene along with the small energy separation of the $T_2 - S_1$ pair suggests that the concept of using the "electron density overlap of the half-occupied orbitals" for estimating the singlet-triplet splittings is general and also holds for alternant conjugated hydrocarbons.

It is evident that in special cases doubly excited closed-shell configurations such as for example H^0L^2 can considerably lower the energy of an excited singlet state. Since such configurations are not present in the triplet wave function due to the Pauli exclusion principle, their admixture reduces the singlet-triplet splitting - an effect beyond the concept of electron density overlap applied here.

It is noteworthy, that the type of molecules where T_1 and S_1 are almost isoenergetic could be of extreme interest for application as light emitting chromophores in OLEDs: In such special molecules, the strong triplet T_1 population which is typically formed in the electron-hole recombination process[2] (mostly due to the trifold degeneracy of the triplet states) can undergo reverse intersystem crossing to S_1 and hence increase the S_1 state population. The delayed fluorescence could lead to a considerable enhancement in the fluorescence quantum yield of OLEDs.

Table 1:

Experimental and theoretical energy values of the electronic states of azulene (all energies in eV). The highest occupied molecular orbital and the lowest unoccupied molecular orbital are abbreviated as H and L. For example, H-1 is then accordingly the orbital below the HOMO. Note that the phase (sign) of the configuration is important to evaluate the corresponding singlet-triplet pairs.

state	ΔE (anion) this work	ΔE (neutral) this work	Literature values	Theory[8] this work	Electron configuration
EA/S_0	0.790	0	0.790[1] 0.71[2]	0.65 eV[9]	
T_1	2.512	1.722	1.677[3], 1.739[4] 1.79[2]	1.758	-0.95 H→L
S_1	2.561	1.771	1.771[5]	1.827	-0.92 H→L
T_2	3.147	2.380	-	2.264	+0.91 H-1→L, -0.27 H→L+1
T_3	3.619	2.852	2.820[6]	2.701	+0.91 H→L+1, +0.28 H-1→L
S_2	4.355	3.565	3.565[7]	3.459	+0.70 H-1→L, -0.60 H→L+1
T_4	4.653	3.863	-	3.871	-0.72 H-1→L+1, -0.59 H-2→L
S_3	-	-	4.200[6]	4.126	-0.68 H-1→L+1, +0.50 H-2→L
T_5	-	-	-	4.379	+0.70 H-2→L, -0.61 H-1→L+1
S_4	-	-	-	4.502	+0.62 H→L+1, +0.52 H-1→L
S_6	-	-	-	5.211	-0.49 H-1→L+1 -0.43 H-2→L -0.56 H-1,H→L^2

1) In the gas phase: Ref. 29
2) Theoretical calculation: Ref: 32
3) In phenazine host crystal: Ref. 27
4) In isopentane: Ref. 28
5) In the gas phase: Ref. 19
6) Electron energy loss spectroscopy: Ref. 11
7) In the gas phase: 30
8) Vertical DFT/MRCI excitation energies at the anion ground-state geometry
9) adiabatic electron affinity (B3-LYP with the TZVPP basis set) with zero-point correction

Figure captions

Figure 1: Structures of naphthalene (a) and azulene (b). If, when going in a counter-clockwise direction, stars are attached to the end of each double bond, all stared atoms have non-stared next neighbors in naphthalene but not in azulene (see the carbon atoms between which the transannular bond is formed). By this definition naphthalene is an alternant conjugated hydrocarbon and azulene is a non-alternant conjugated hydrocarbon. For further explanation see text.

Figure 2: Photodetachment photoelectron spectrum of azulene. Beside the extensively well investigated transitions to the S_1 and S_2 states, the transitions to the T_1, T_2, T_3 and T_4 states are observed. The inset g) shows the expanded T_1-S_1 splitting. The right inset f) shows the transitions to T_2 and T_3 recorded with higher electron transmission and lower electron energy resolution. For the explanations of the sections a)-e), the assignments and further interpretations, see text. The experimental origin peak positions are presented in Table 1.

Figure 3 a, b): Comparison of Franck-Condon simulated and experimental vibronic spectra of anion-to-neutral transitions. Shown are vibronic spectra of the anion-to-S_0 (a) and anion-to-S_2 transitions b). Note especially the very good agreement of the simulated and experimental spectra for the S_0 state. The simulated Franck-Condon spectrum of the S_2 state clearly shows, that the peak at 298 meV (referred to the S_2 origin position) is not a vibration, but a separate electronic origin transition. For further explanation see text.

Figure 3 c, d): Comparison of Franck-Condon simulated and experimental vibronic spectra of anion-to-neutral transitions: c) The Franck-Condon simulated spectra of T_1 and S_1 (note the T_1-S_1 energy shift, as observed in the experiment). d) The calculated and measured vibronic spectra for the anion to T_1 and S_1 transitions. The two theoretical spectra of T_1 and S_1 have been shifted and added for better comparison to the experiment. For further explanations, see text.

Figure 4: DFT/MRCI electronic state energies along an interpolated reaction coordinate (RC) between the S_0 state equilibrium structure and the crossing points of the T_2 state with the T_1 and the S_1 states. Note that the T_1 and S_1 potentials are very close and almost parallel to each other. Note also that T_1 and S_1 are very shallow along this path. For further explanation see text.

Figure 5: Frontier orbitals of azulene: (a) LUMO+1, (b) LUMO, (c) HOMO, (d) HOMO-1 and (e) HOMO-2. Each of the plotted surfaces encases 95 % of the total orbital electron density. In azulene, the S_1 and T_1 states have predominantly $HOMO^1$-$LUMO^1$ electron configurations. The electron densities of these two orbitals (see b and c) are almost disjunct. Please note that for the electron densities the phases of the wave functions are of no importance. For further explanation, see text.

Figure 6: Electron wave functions of the frontier orbitals of naphthalene: (a) LUMO+1, (b) LUMO, (c) HOMO and (d) HOMO-1. Each of the plotted surfaces encases 95 % of the total orbital electron density. In naphthalene, S_2 and T_1 have predominantly $HOMO^1$-$LUMO^1$ electron configurations and form a singlet-triplet pair. Note that the electron densities of these two orbitals strongly overlap (compare b) and c)). S_1 and T_2 form also a singlet-triplet pair. They have both about equal contributions of $(H-1)^1L^1$ and $H^1L+1)^1$ configurations. Note that the electron density overlaps between a) and c) as well as between d) and b) are relatively small. For further explanation, see text.

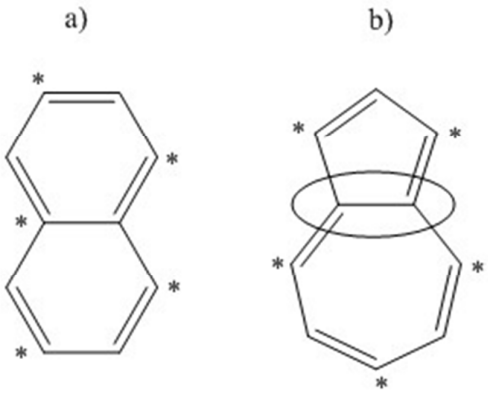

Figure 1: Structures of naphthalene (a) and azulene (b). If, when going in a counter-clockwise direction, stars are attached to the end of each double bond, all stared atoms have non-stared next neighbors in naphthalene but not in azulene (see the carbon atoms between which the transannular bond is formed). By this definition naphthalene is an alternant conjugated hydrocarbon and azulene is a non-alternant conjugated hydrocarbon. For further explanation see text.

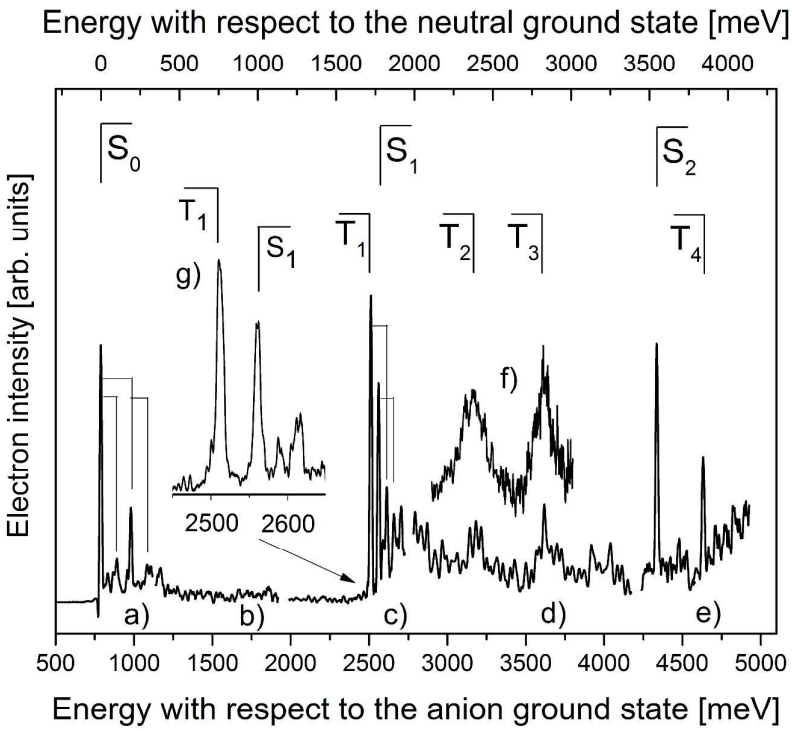

Figure 2: Photodetachment photoelectron spectrum of azulene. Beside the extensively well investigated transitions to the S_1 and S_2 states, the transitions to the T_1, T_2, T_3 and T_4 states are observed. The inset g) shows the expanded T_1-S_1 splitting. The right inset f) shows the transitions to T_2 and T_3 recorded with higher electron transmission and lower electron energy resolution. For the explanations of the sections a)-e), the assignments and further interpretations, see text. The experimental origin peak positions are presented in Table 1.

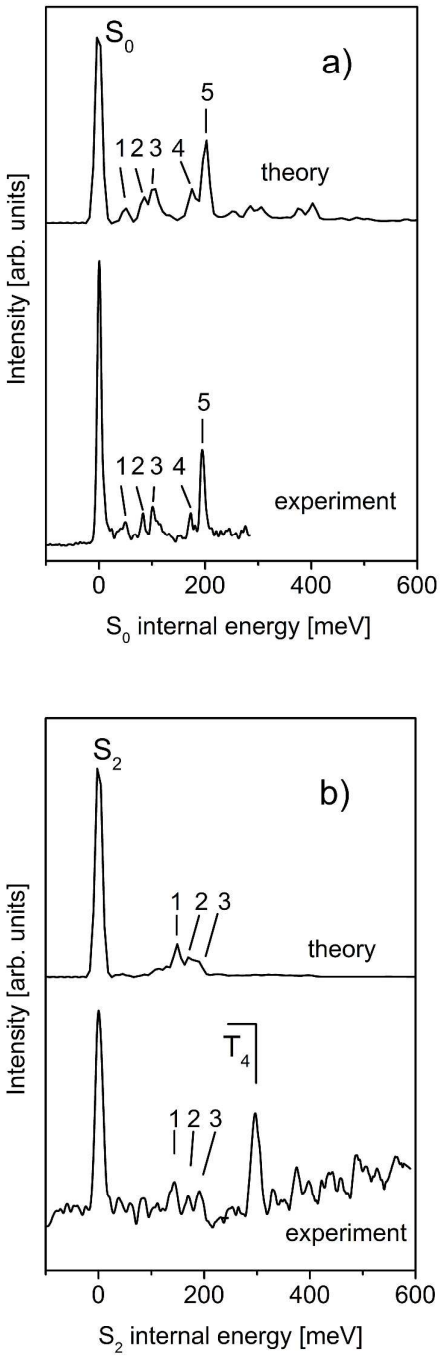

Figure 3 a,b): Comparison of Franck-Condon simulated and experimental vibronic spectra of anion-to-neutral transitions. Shown are vibronic spectra of the anion-to-S_0 (a) and anion-to-S_2 transitions b). Note especially the very good agreement of the simulated and experimental spectra for the S_0 state. The simulated Franck-Condon spectrum of the S_2 state clearly shows, that the peak at 298 meV (referred to the S_2 origin position) is not a vibration, but a separate electronic origin transition. For further explanation see text.

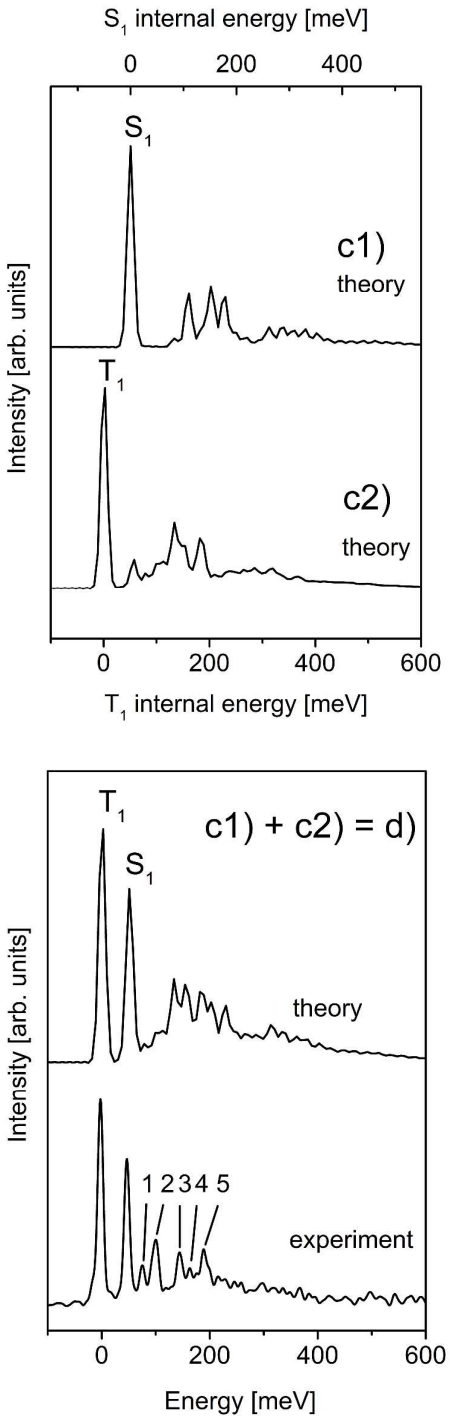

Figure 3 c, d): Comparison of Franck-Condon simulated and experimental vibronic spectra of anion-to-neutral transitions: c) The Franck-Condon simulated spectra of S_1 (c1) and T_1 (c2). The energy shift between the simulated spectra corresponds to the T_1-S_1 splitting taken from the experiment. d) The calculated (c1+c2) and measured vibronic spectra for the anion to T_1 and S_1 transitions. For further explanations, see text.

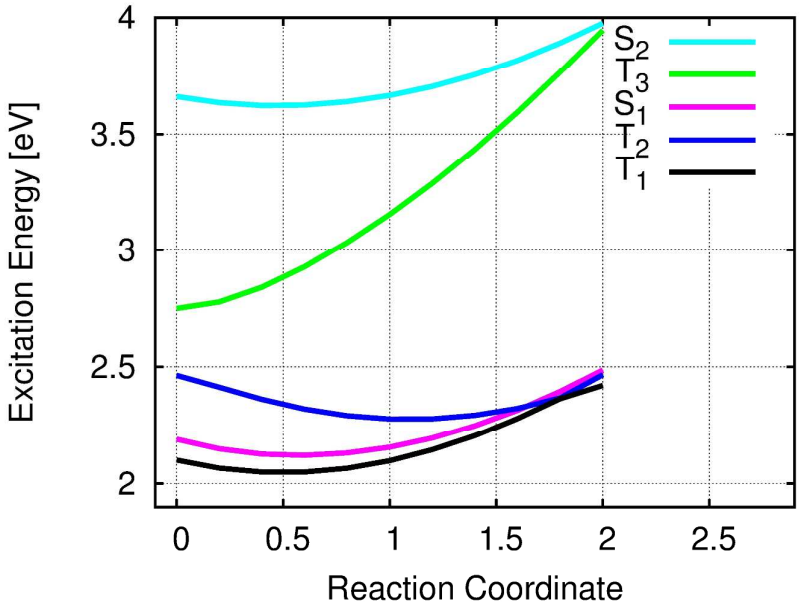

Figure 4: DFT/MRCI electronic state energies along an interpolated reaction coordinate (RC) between the S_0 state equilibrium structure and the crossing points of the T_2 state with the T_1 and the S_1 states. Note that the T_1 and S_1 potentials are very close and almost parallel to each other. Note also that T_1 and S_1 are very shallow along this path. For further explanation see text.

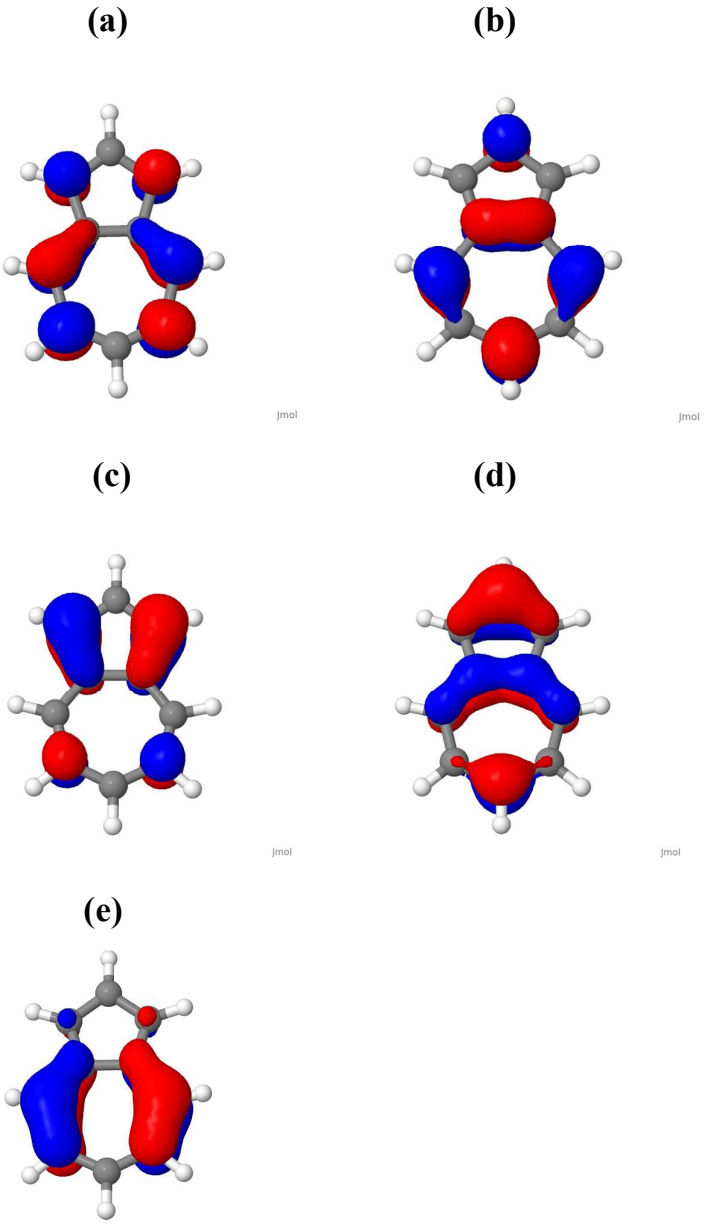

Figure 5: Frontier orbitals of azulene: (a) LUMO+1, (b) LUMO, (c) HOMO, (d) HOMO-1 and (e) HOMO-2. Each of the plotted surfaces encases 95 % of the total orbital electron density. In azulene, the S_1 and T_1 states have predominantly $HOMO^1$-$LUMO^1$ electron configurations. The electron densities of these two orbitals (see b and c) are almost disjunct. Please note that for the electron densities the phases of the wave functions are of no importance. For further explanation, see text.

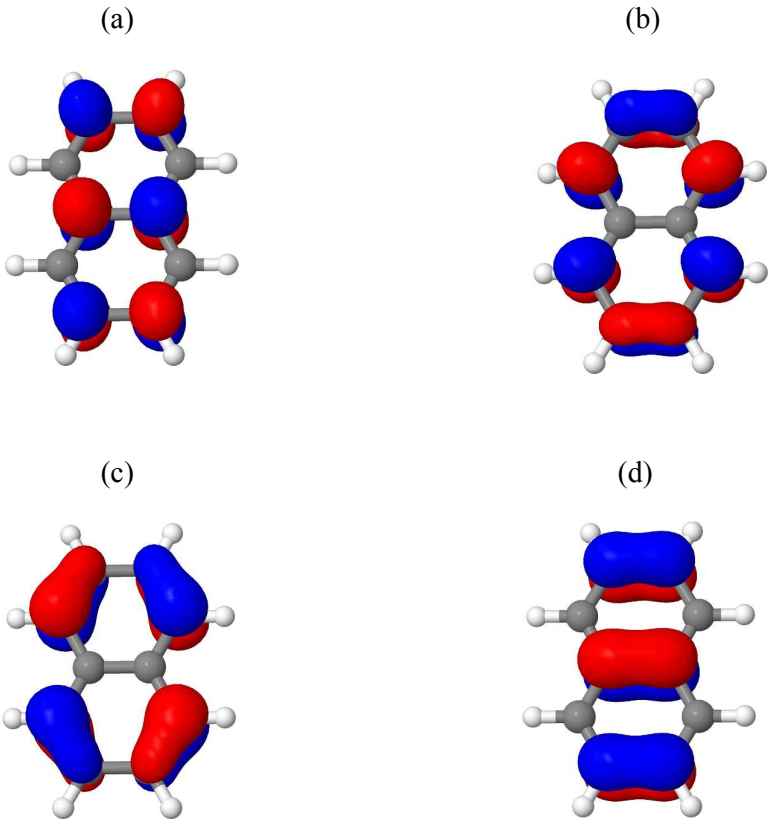

Figure 6: Electron wave functions of the frontier orbitals of naphthalene: (a) LUMO+1, (b) LUMO, (c) HOMO and (d) HOMO-1. Each of the plotted surfaces encases 95 % of the total orbital electron density. In naphthalene, S_2 and T_1 have predominantly $HOMO^1$-$LUMO^1$ electron configurations and form a singlet-triplet pair. Note that the electron densities of these two orbitals strongly overlap (compare b) and c)). S_1 and T_2 form also a singlet-triplet pair. They have both about equal contributions of $(H-1)^1L^1$ and $H^1L+1)^1$ configurations. Note that the electron density overlaps between a) and c) as well as between d) and b) are relatively small. For further explanation, see text.

References

1 *Modern Molecular Photochemistry of Organic Molecules,* Ed.: N. J. Turro, V. Ramamurthy, J.C. Scaiano, University Science Books, Sausalito, 2010.

2 A. Köhler and H. Bässler, *Mat. Sci. Eng. R.*, 2009, **66**, 71-109.

3 Y. Tomkiewitcz, R.P. Groff, and P. Avakian, *J. Chem. Phys*. 1971, **54**, 4504-4507.

4 G.V. Maier, V.I. Danilova, *Quantum Chemistry*, *Structure*, *and Photonics* of *Molecules*, Tomsk State University, Tomsk, 1984, **218,** 11.

5 W. Leupin and J. Wirz, *J. Am. Chem. Soc.* 1980, **102**, 6068-6075.

6 M. Allan, *J. of Electron Spec. and Related Phen.*, 1989, **48**, 219-351.

7 S. Siegert, F. Vogeler, C.M. Marian, and R. Weinkauf, *Phys. Chem. Chem. Phys*. 2011, **13**, 10350-10363.

8 F. Vogeler, S. Siegert, C. M. Marian, and R. Weinkauf, *Chem. Phys. Chem.* 2011, **12**, 1948-1956.

9 C.A. Coulson and G.S. Rushbrooke, *Proc. Camb. Philos. Soc.* 1940, **36**, 193-200.

10 *The PMO Theory of Organic Chemistry*, Ed.: M.J.S. Dewar and R.C. Dougherty, Plenum Press, New York, 1975, page 73 ff.

11 *Photochemistry of Organic Compounds: From Concepts to Practice*, Ed.: P. Klan, J. Wirz, John Wiley&Sons, Weinheim, 2009, page 151 ff.

12 D.L. Dexter, *J. Chem. Phys.,* 1953, **21**, 836-850.

13 *Modern Quantum Chemistry: Introduction to advanced electronic structure theory*, Ed.: A. Szabo and N.S. Ostlund, Dover Publications, New York, 1996

14 M. Kasha, Discuss. *Faraday Soc.,* 1950, **9**, 14-19.

15 M. Beer and H.C. Longuet-Higgins, *J. Chem. Phys.*, 1955, **23**, 1390-1391.

16 G. Viswanath and M. Kasha, *J. Chem. Phys.*, 1956, **24**, 574-577.

17 R. Engelman and J. Jortner, *Molecular Physics*, 1970, **18**, 145-164.

18 D. Huppert, J. Jortner, and P.R. Rentzepis, *J. Chem. Phys.,* 1972, **56**, 4826-4833.

19 T. Suzuki and M. Ito, *J. Phys. Chem.*, 1987, **91**, 3537-3542.

20 E.W.-G. Diau, S. de Feyter, and A.H. Zewail, *J. Chem. Phys*., 1999, **110**, 9785-9788.

21 M.J. Bearpark, F. Bernardi, S. Clifford, M. Olivucci, M.A. Robb, B.R. Smith, and T. Vreven, *J. Am. Chem. Soc.,* 1996, **118**, 169-175.

22 S. Klein, M. J. Bearpark, B.R. Smith, M.A. Robb, M. Olivucci, and F. Bernardi, *Chem. Phys. Lett*., 1998, **292**, 259-266.

23 A.A. Ruth, E.-K. Kim, and A. Hese, *Phys. Chem. Chem. Phys*., 1999, **1**, 5121-5128.

24 A.J. Wurzer, T. Wilhelm, J. Piel, and E. Riedle, *Chem. Phys. Lett*., 1999, **299**, 296-302.

25 Y.Niu, Q. Peng, C. Deng, X. Gao, and Z. Shuai, *J. Phys. Chem.,* A, 2010, **114**, 7817-7831.

26 M. Dierksen and S. Grimme, *J. Chem. Phys*., 2004, **120**, 3544-3554.

26

27 D. Klemp and B. Nickel, *Chem. Phys.*, 1983, **78**, 17-28.

28 B. Nickel and D. Klemp, *Chem. Phys.*, 1993, **174**, 297-318.

29 J. Schiedt, W.J. Knott, K. Le Barbu, E.W. Schlag, and R. Weinkauf, *J. Chem. Phys.*, 2000, **113**, 9470-9478.

30 Y. Semba, K. Yoshida, S. Kasahara, C. Ni, Y. Hsu, S. H. Lin, Y. Ohshima, and M. Baba, *J. Chem. Phys.*, 2009, **131**, 024303-1-6.

31 O.C. Hofer and R.M. Hedges, *Chem. Phys. Lett.,* 1970, **6**, 67-71.

32 M. Huzak, B. Hajgató, and M.S. Deleuze, *Chem. Phys*. 2012, **406**, 55-64.

33 TURBOMOLE, a development of the University of Karlsruhe and the Forschungszentrum Karlsruhe GmbH, 1989-2007, TURBOMOLE GmbH, since 2007; available from http://www.turbomole.com

34 A.D. Becke, *J. Chem. Phys*., 1993, **98**, 5648-5652.

35 C. Lee, W. Yang, and R.G. Parr, *Phys. Rev. B,* 1988, **37**, 785-789.

36 F. Furche and R. Ahlrichs, *J. Chem. Phys.,* 2002, **117,** 7433-7447.

37 a) A. Schäfer, C. Huber, and R. Ahlrichs, *J. Chem. Phys.*, 1994, **100**, 5829-5835.
b) F. Weigend, M. Häser, H. Patzelt, and R. Ahlrichs, *Chem. Phys. Lett*., 1998, **294**, 143-152.

38 J**.** Neugebauer, M. Reiher, C. Kind, and B. A. Hess, *J. Comput. Chem.,* 2002, **23**, 895-910.

39 M. Etinski, J. Tatchen, and C. M. Marian, *Phys. Chem. Chem. Phys.*, 2014, **16**, 4740-4751.

40 S. Grimme and M. Waletzke, *J. Chem. Phys.,* 1999, **111**, 5645-5655.

41 A. D. Becke, *J. Chem. Phys*., 1993, **98**, 1372-1377.

42 J. Schiedt and R. Weinkauf, *Rev. Sci. Instrum*., 1999, **70**, 2277-2281.

43 E.P. Wigner, *Phys. Rev.*, 1948, **73**, 1002-1009.

44 J. Schiedt and R. Weinkauf, *J. Chem. Phys*., 1999, **110**, 304-314.

45 D. Tanaka, S. Sato, and K. Kimura, *Chem. Phys.,* 1998, **239**, 437-445.